Knockdown of MIR9-3HG inhibits proliferation and promotes apoptosis of cervical cancer cells by miR-498 via EP300

FANG LI[1], YING LIANG[2] and PIAN YING[3]

[1]Gynaecology Department, Jiangxi Maternal and Child Health Hospital, Nanchang, Jiangxi 330006; [2]Gynecology Department, Jiangxi University of Traditional Chinese Medicine, Nanchang, Jiangxi 330004; [3]Department of Gynecology and Obstetrics, The First Affiliated Hospital of Zhejiang Chinese Medical University, Hangzhou, Zhejiang 310006, P.R. China

Received August 12, 2020; Accepted February 12, 2021

DOI: 10.3892/mmr.2021.12388

Abstract. Cervical cancer is a serious gynecological cancer and one of the primary causes of mortality in female patients with cancer. Despite advances in cancer research, the molecular mechanism underlying cancer remains poorly understood. High levels of MIR9-3 host gene (HG) are associated with the occurrence and development of cervical cancer. However, the specific role of MIR9-3HG during the development of cervical cancer is unclear. In the present study, the expression of MIR9-3HG was silenced in C33A and SiHa cervical cancer cell lines. Proliferation and apoptosis were measured in these cells using 5-ethynyl-2'-deoxyuridine assay and flow cytometry, respectively. In addition, targeting microRNAs (miRs) of MIR9-3HG and mRNAs of miR-498 were predicted using public databases. The predicted interactions between these molecules were validated using RNA immunoprecipitation, RNA pull-down and luciferase reporter assays. Lastly, C33A cells transfected with short hairpin MIR-3HG alone or in combination with miR-498 inhibitor or PC-EP300 were subcutaneously injected into mice. The levels of miR-498, EP300 and Ki67 in tumor tissue were measured via reverse transcription-quantitative PCR or western blotting. MIR9-3HG knockdown inhibited the proliferation of cervical cancer cells, whilst promoting apoptosis. MIR9-3HG sponged miR-498 and inhibited its expression. Additionally, miR-498 interacted with EP300 and inhibited its expression. Transfection with miR-498 inhibitor significantly decreased apoptosis levels; this effect was abolished following EP300 silencing *in vitro*. *In vivo*, both miR-498 inhibition and EP300 overexpression reversed the inhibition of tumor growth mediated by MIR-3HG knockdown. MIR9-3HG promoted the proliferation cervical cancer cells via EP300 and miR-498. These *in vitro* and *in vivo* findings demonstrate the regulatory role of the MIR9-3HG/miR-498/EP300 axis in cervical cancer cell growth. Thus, the present study identified novel molecular targets for the diagnosis and treatment of cervical cancer and provided new insight into the pathogenesis of cervical cancer.

Correspondence to: Dr Pian Ying, Department of Gynecology and Obstetrics, The First Affiliated Hospital of Zhejiang Chinese Medical University, 54 Youdian Road, Shangcheng, Hangzhou, Zhejiang 310006, P.R. China
E-mail: pianyingp@163.com

Key words: cervical cancer, MIR9-3 host gene, microRNA-498, EP300, proliferation, apoptosis

Introduction

Cervical cancer is a common gynecological malignant tumor with a high mortality rate. There are 530,000 newly diagnosed cases of cervical cancer worldwide and >270,000 deaths each year (1). The diagnosis of early and mid-stage cervical cancer is increasingly accurate, and patient prognosis has improved (2,3). However, cervical cancer remains the leading cause of morbidity and mortality among women worldwide.

Previous studies have demonstrated that non-coding RNA serves an important role in physiological functions (4,5), such as metabolism, differentiation and apoptosis of various types of cell (6). Certain studies have suggested that the expression of microRNA (miRNA or miR) is associated with the occurrence and development of diverse types of cancer, such as breast cancer and thyroid cancer (7,8). Long non-coding RNA (lncRNA) sponges miRNA and decreases miRNA levels, thereby regulating downstream target genes (9). This lncRNA/miRNA/mRNA axis has been implicated in the regulation of biological processes in cancer cells, such as osteosarcoma (10,11).

A previous study indicated that the expression of MIR9-3 host gene (HG) is a biomarker of the development of cervical cancer (12). Additionally, MIR9-3HG is upregulated in head and neck squamous cell carcinoma tissue (13). However, whether MIR9-3HG affects the proliferation and metastasis of cervical cancer cells is unclear.

The present study investigated the expression of MIR9-3HG and its potential regulatory role in the proliferation of cervical cancer cells *in vitro*. Cancer cell apoptosis was detected via flow cytometry. The potential molecular mechanism of action of MIR9-3HG was further investigated by screening bioinformatics databases, then validated via *in vitro* and *in vivo* experiments. The aim of the study was to provide insight

into the role of MIR9-3HG in the proliferation and apoptosis of cervical cancer cells, as well as the underlying molecular mechanism.

Materials and methods

Cell culture and treatment. Cervical cancer cell lines (cervical squamous cell carcinoma, C33A; human papillomavirus-related cervical squamous cell carcinoma, SiHa; human papillomavirus-related endocervical adenocarcinoma, HeLa; human papillomavirus-related cervical squamous cell carcinoma, CaSki; and human cervical epithelial immortalized cells, H8 (used as normal control group.) were obtained from the Chinese Academy of Sciences (Shanghai, China). All cell lines were cultured with RPMI-1640 medium (HyClone; Cytiva) supplemented with 10% fetal bovine serum (FBS; Gibco; Thermo Fisher Scientific, Inc.) at 37˚C in a humidified atmosphere with 5% CO_2. MIR9-3HG and EP300 knockdown and ER300 overexpression were performed in C33A and SiHa cells using plasmids. The miR-498 inhibitor and mimic were purchased from Shanghai GeneChem Co., Ltd. Polybrene was obtained from Shanghai GeneChem Co., Ltd. and used to enhance transfection efficacy.

Lentivirus, plasmids and miR-mimic or miR-inhibitor transfection. MIR9-3HG and EP300 knockdown lentiviral vectors, as well as EP300 overexpression pcDNA3.1 plasmids were obtained from Shanghai GeneChem Co., Ltd. A total of $3x10^6$ 293T cells were seeded into a 10-cm cell culture dish and cultured overnight at 37˚C with 5% CO_2. The lentivirus was packaged and prepared by transfecting vectors into 293T cells (American Type Culture Collection). The ratio of the lentiviral plasmid:packaging vector was 4:3:1.

The lentivirus was collected, then transduced into C33A or SiHa cells (lentivirus titer 2x10 TU/ml) using polybrene (Beijing Solarbio Science & Technology Co., Ltd.). The miR-498 inhibitor (120 nM; 5'-CUUUUUGCGGGGGACCGAACUUU-3'), miR-498 mimic (40 nM; 5'-GAAAAACGCCCCCUGGCUUGAAA-3') and their negative controls (NC; random sequence anti-miR molecule and scrambled miRNA, respectively) were transfected into C33A or SiHa cells using Lipofectamine® 3000 (Thermo Fisher Scientific, Inc.) at room temperature for 48 h.

Cell Counting Kit (CCK)-8 assay. CCK-8 assay was performed to evaluate the cell viability. C33A and SiHa cells ($2x10^4$ cells/ml) were plated into four 96-well plates and cultured at 37˚C. After 24, 48 or 72 h transfection, CCK-8 reagent (10 μl) (Dojindo Molecular Technologies, Inc.) was added into culture medium and added into the 96-well plates. The cells were incubated for 1 h. After incubation, absorbance at 450 nm was measured using a spectrophotometer (Thermo Fisher Scientific, Inc.).

5-Ethynyl-2'-deoxyuridine (Edu) assay. The proliferation of C33A and SiHa cells was evaluated via EdU assay (Yusheng Company; https://www.yeasen.com/search?q=EdU), according to the manufacturer's instructions. The nuclei were stained with DAPI for 5 min at room temperature in the dark according to manufacturer' protocol (Sigma-Aldrich; Merck KGaA).

Apoptosis assay. Apoptosis rates were determined using commercial kits (Beyotime Institute of Biotechnology). Cells were washed in PBS to remove FBS, then incubated with Annexin-V and PI for 40 min at 4˚C in the dark. The apoptosis rate was detected via flow cytometry (Attune NxT; Thermo Fisher Scientific, Inc.). The ratio of early and late stage apoptosis was expressed as Q2+Q3. The apoptosis levels were analyzed with FlowJo 10 software (Becton, Dickinson and Company).

Reverse transcription-quantitative (RT-q)PCR. Total RNA of C33A and SiHa cells or nude mice tissues was collected using TRIzol® at room temperature (Thermo Fisher Scientific, Inc.). RNA was reverse transcribed into cDNA using an RT kit (Takara Bio, Inc.) at 42˚C for 60 min, followed by transcription at 70˚C for 5 min. Amplification of cDNA was performed using the ABI 7500 system (Thermo Fisher Scientific, Inc.). For the detection for miR-498 levels, miRNA was extracted using Rapid Extraction kit for miRNA (HaiGene; http://www.haigene.cn/) and then reverse transcribed using TaqMan miRNA RT kit. The quantification for miR-498 was performed using TaqMan miRNA qPCR kit (HaiGene; http://www.haigene.cn/) and U6 was used as the internal reference. The qPCR thermocycling conditions were as follows: Initial denaturation at 95˚C for 5 min, followed by 35 of cycles of denaturation at 95˚C for 30 sec, annealing at 56.2˚C for 30 sec and extension at 72˚C for 30 sec; followed by a final extension at 72˚C for 7 min. The results were analyzed via the $2^{-\Delta\Delta Cq}$ method (14). The primers used were as follows: MIR9-3HG forward, 5'-CAGATGTTCGGTCCCCACTC-3' and reverse, 5'-TCGGCCTCCTTTGCTTAGAC-3'; miR-498 forward, 5'-GGTTTGAAGCCAGGCGGTTTC-3' and reverse, 5'-CAGTGCAGGGTCCGAGGTAT-3'; cysteine and histidine rich domain containing 1 (CHORDC1) forward, 5'-CATGCACCACTACACTCAGC-3' and reverse, 5'-GCCTCCTTGCTGACTGATTC-3'; eukaryotic translation initiation factor 3 subunit J (EIF3J) forward, 5'-CGGAGCAGCAGGAAATCTCT-3' and reverse, 5'-GCAGGTTTTGTTGCGAAGTG-3'; EP300 forward, 5'-AAAAATAAGAGCAGCCTGAG-3' and reverse, 5'-AGACCTCTTTATGCTTCTTCC-3'; lectin, mannose binding 1 (LMAN1) forward, 5'-GCACAAGGGCATTTTGGA-3' and reverse, 5'-GAAAGGACATCATGGTCATCTG-3'; GRIP and coiled-coil domain-containing protein 2 (GCC2) forward, 5'-AGCTTCAGAAAACCATGCAAGAA-3' and reverse, 5'-GCTCAGCTTGTACTCAGGGC-3'; DEAH-box helicase 35 (DHX35) forward, 5'-TACACCTACACCGGCAAAAGC-3' and reverse, 5'-AAAACAGCTCCGCATCAACCT-3'; GAPDH forward, 5'-GGAGCGAGATCCCTCCAAAAT-3' reverse, 5'-GGCTGTTGTCATACTTCTCATGG-3' and U6 forward, 5'-CGGGTTTGTTTTGCATTTGT-3' and reverse, 5'-AGTCCCAGCATGAACAGCTT-3'. The detection of expression of MIR9-3HG in the cytoplasm and nucleus was performed using commercial kits Cytoplasmic & Nuclear RNA Purification Kit (50) (cat. no. 21000; Norgen Biotek Corp.) according to the manufacturer's instructions.

Western blotting. Total protein of C33A cells, SiHa cells or tumor tissue of nude mice was collected using RIPA buffer (Beyotime Institute of Biotechnology). Protein concentration was determined using the BCA method (Beyotime

Institute of Biotechnology). Proteins (50 μg) of each lane were separated on 10% SDS-PAGE gels (Beyotime Institute of Biotechnology), then transferred to PVDF membranes (EMD Millipore). Following blocking with 5% skimmed milk (Thermo Fisher Scientific, Inc.) for 2 h at 4˚C, the membranes were incubated with primary antibodies (all Abcam) at 4˚C overnight. The primary antibodies used were specific for EP300 (cat. no. ab10485; 1:5,000), Ki-67 (cat. no. ab92742; 1:5,000) and GAPDH (cat. no. ab9485; 1:2,500). After incubation, the membranes were washed in PBST containing 0.05% Tween-20, then incubated with secondary antibodies (goat anti Rabbit IgG; cat. no. ab216777; 1:10,000). Protein bands were visualized using enhanced chemiluminescence reagent (Pierce; Thermo Fisher Scientific, Inc.) and then analyzed using ImageJ software 1.46r (National Institutes of Health).

RNA immunoprecipitation assay (RIP). RIP was performed using commercial kits (EZ-Magna RIP™ RNA-Binding Protein Immunoprecipitation kit; EMD Millipore), according to the manufacturer's instructions. pSL-MS2-12X (Addgene, Inc.), together with pcDNA3.1 or pcDNA3.1- MIR9-3HG (Genomeditech), was used to construct pcDNA3.1-MS2-12X (2 μg) or pcDNA3.1- MIR9-3HG-MS2-12X vectors, which were then co-transfected into C33A or SiHa cells with pMS2-GFP (Addgene, Inc.) using Lipofectamine 3000 (Thermo Fisher Scientific, Inc.) at room temperature. After 48 h, the transfected cells were collected for RIP. Briefly, cells were lysed in Complete RIP lysis buffer containing RIP Lysis Buffer, Protease Inhibitor Cocktail and RNase Inhibitor (Guangzhou Sai Cheng Biotechnology Co., Ltd.) for 5 min. Magnetic beads were resuspended in RIP Wash Buffer and mixed with anti-GFP or IgG (5 μg; GFP, cat. no. 11814460001; IgG, cat. no. 06681743001; Roche Diagnostics). Following incubation at room temperature for 30 min, the RIP Buffer was added to the magnetic bead and antibody mixture, followed by the cell lysate. Following incubation overnight at 4˚C, the precipitate was collected and resuspended in Proteinase K Buffer (150 μl). The miRNA enriched by IP was reverse-transcribed to cDNA for RT-qPCR analysis, as described previously.

RNA pull-down assay. Biotin-labeled RNA probes [lncRNA full-length or mutant (Mut)] were obtained through *in vitro* transcription. The pSP72 plasmid (Addgene, Inc.) containing full-length wild-type (WT) or Mut MIR-3HG was digested using a single enzyme to obtain a linear template, which was then labeled using Biotin RNA Labeling Mix (Roche Diagnostics). The biotin-labeled RNA (3 μg) was added to cell lysate prepared using 1 ml TRIzol (Takara Bio, Inc.), then incubated at room temperature for 1 h. The RNA mixture (100 μg) was then mixed with magnetic beads labeled by streptavidin according to manufacturer's protocol for 1 h (Dyna beads M-280 Streptavidin; Thermo Fisher Scientific, Inc.). After 60 min, the magnetic beads were deposited with a magnetic field holder and then the supernatant was discarded Then, the beads were washed three times with lysis buffer. The beads were re-suspended in Elution Buffer (15 μl) at 70˚C. The magnetic beads were deposited with a magnetic field holder to collect the supernatant for RT-qPCR analysis of miR-498 expression levels as described previously.

Bioinformatic prediction. The expression of MIR9-3HG in cervical tumor and normal tissue was analyzed using the Gene Expression Profiling Interactive Analysis (GEPIA) database (cervical tumor number =306; normal number =13; gepia.cancer-pku.cn/). The targeting miRNAs were predicted using the PITA (genie.weizmann.ac.il/pubs/mir07/mir07_dyn_data.html), DIANA-microT (diana.cslab.ece.ntua.gr/microT) and miRNAMAP (mirnamap.mbc.nctu.edu.tw) databases. The association of miR-498 or EP300 with MIR9-3HG was predicted through Starbase v2.0 (http://starbase.sysu.edu.cn/).

Dual luciferase assay. Luciferase assays were performed using Pierce™ *Renilla*-Firefly Luciferase Dual Assay kit (Thermo Fisher Scientific, Inc.), according to the manufacturer's instructions. Transient plasmid transfection was performed when the cells reached 70-80% confluence. The miR-498 mimic was co-transfected into C33A or SiHa cells together with MIR9-3HG-WT-1, MIR9-3HG-WT-2, MIR9-3HG-Mut-1,MIR9-3HG-Mut-2,MIR9-3HG-WT-1-WT-2, MIR9-3HG-WT-1-Mut-2, MIR9-3HG-WT-2-Mut-1 or MIR9-3HG-Mut-1-Mut-2 luciferase reporter plasmid (Promega Corporation) using Lipofectamine® 2000 (Thermo Fisher Scientific, Inc.) at 37˚C for 48 h. After discarding medium, the cells were washed with PBS 2-3 times. Then, 100 μl lysis buffer was added to each well and incubated in an orbital shaker in a cold room for ~20 min to fully lyse the cells. Luciferase activity was analyzed using a luminometer fluorescence detector (Turner BioSystems; Thermo Fisher Scientific, Inc.). *Renilla* luciferase activity was used as internal reference.

Animal experiments. A total of 18 female nude mice (age, 4-6 weeks; weight, 16-18 g) were obtained from the Shanghai Experimental Animal Center, Chinese Academy of Sciences (Shanghai, China). The cage tools, feed, padding and drinking water used were sterilized by high pressure steam and handled by professionals. The room had a 12-h light/dark cycle, a temperature of 25-27˚C and a relative humidity of 40-45%. The mice had free access to food and water.

C33A cells were re-suspended with PBS ($5x10^6$ cells/ml). C33A cells (0.2 ml) in each experimental group (n=3 mice) were injected subcutaneously into in the right armpit of nude mice. Vernier calipers were used to measure tumor volume every three days for three weeks. After three weeks, mice were sacrificed by cervical dislocation. Death was indicated by cessation of breathing, muscle relaxation and lack of nerve reflex. The tumor tissue was weighed using electronic scales. The experiment lasted for 21 days and there was no mouse death during experiment. The animal health and behavior were monitored every day. The experiments were approved by the Ethics Committee of the First Affiliated Hospital of Zhejiang Chinese Medical University.

Statistical analysis. All data were analyzed using GraphPad Prism 7.0 software (GraphPad Software, Inc.). Data are presented as the mean ± SD (n=3). The comparison between groups was performed by one-way ANOVA, followed by Tukey's post hoc test. $P<0.05$ was considered to indicate a statistically significant difference.

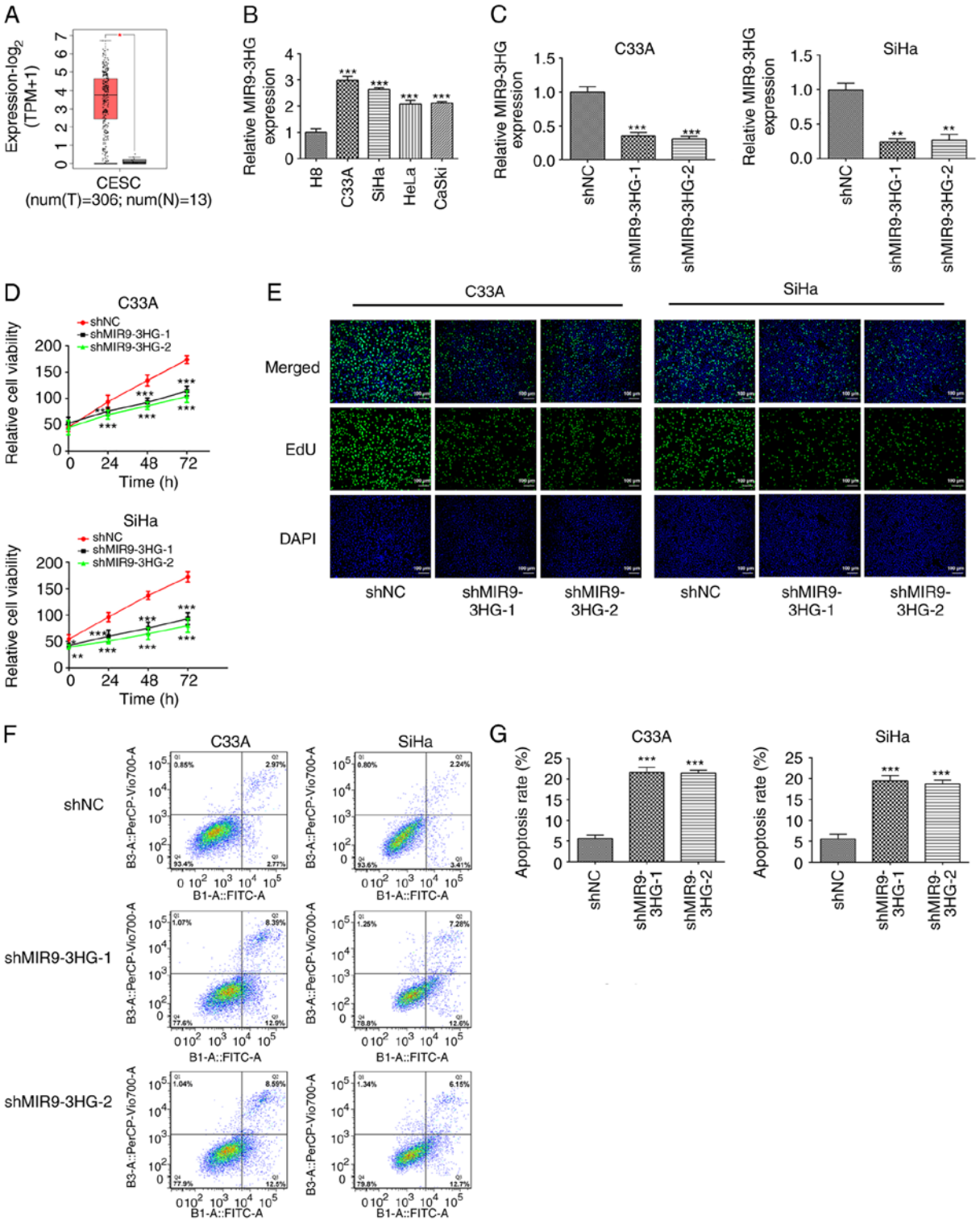

Figure 1. Knockdown of MIR9-3HG suppresses proliferation and promotes apoptosis of cervical cancer cells. (A) Expression levels of MIR9-3HG in cervical cancer and normal tissue from The Cancer Genome Atlas database. *P<0.05. (B) RT-qPCR was performed to detect the expression levels of MIR9-3HG in cervical cancer cell lines. ***P<0.001 vs. H8. (C) RT-qPCR was performed to detect the expression levels of MIR9-3HG in cells of knockdown groups. **P<0.01, ***P<0.001 vs. shNC. Cell (D) viability, (E) proliferation and (F and G) apoptosis were detected via Cell Counting Kit-8 and EdU assays and flow cytometry, respectively. Magnification, x100. Data are presented as the mean ± SD. *P<0.05, **P<0.01, ***P<0.001 vs. shNC. MIR9-3HG, MIR9-3 host gene; RT-q, reverse transcription-quantitative; shNC, short hairpin negative control; EdU, 5-ethynyl-2'-deoxyuridine; T, tumor; N, normal; CESC, cervical squamous cell carcinoma and endocervical adenocarcinoma.

Results

MIR9-3HG knockdown inhibits proliferation and promotes apoptosis of cervical cancer cells. The data obtained from GEPIA database (which contains information from The Cancer Genome Atlas database) showed that the expression of MIR9-3HG in cervical tumor tissue was significantly higher than that in adjacent normal tissue (4-fold difference; Fig. 1A).

The expression of MIR9-3HG in cell lines was determined using RT-qPCR. The expression of MIR9-3HG in cervical cell lines was higher than that in cervical epithelial cells (2.9-fold difference; Fig. 1B). Additionally, the expression levels of MIR9-3HG in C33A and SiHa cells appeared to be higher compared with those in HeLa or CaSki cells. Therefore, C33A and SiHa cells were selected for subsequent experiments and MIR9-HG was silenced in both cell lines. The expression of MIR9-3HG decreased 2.8-fold following knockdown (Fig. 1C). CCK-8 assays were then performed to detect cell viability. Viability of C33A and SiHa cells was inhibited following knockdown of MIR9-3HG (Fig. 1D). Next, cell proliferation was determined via EdU assay. The proliferation of C33A and SiHa cells was inhibited following MIR9-3HG knockdown (Fig. 1E). Flow cytometry was used to measure the apoptosis rates in these cells. The apoptosis rates of C33A and SiHa cells following MIR9-3HG knockdown were significantly increased (4.2-fold; Fig. 1F and G).

MIR9-3HG interacts with miR-498. In order to investigate the molecular mechanism of MIR9-3HG in the pathogenesis of cervical cancer, the distribution of MIR9-3HG was measured in the cytoplasm and nucleus of C33A and SiHa cells. MIR9-3HG was primarily distributed in the cytoplasm of C33A and SiHa cells (Fig. 2A). Using Starbase, MIR9-3HG was demonstrated to interact with multiple miRNAs. RIP assay was then performed to confirm the interaction between MIR9-3HG and these miRNAs. MIR9-3HG overexpression resulted in greater miR-498 enrichment compared with the control (Fig. 2B), indicating an interaction between MIR9-3HG and miR-498. This was also confirmed via RNA pull-down assay. The enrichment in miR-498 was decreased 5.9-fold in C33A or SiHa cells with MIR9-3HG-Mut, compared with the Biotin-labeled MIR9-3HG WT group (Fig. 2C).

miR-498 was then overexpressed in C33A and SiHa cells. The expression of miR-498 was increased in the overexpression group, compared with NC (2.9-fold difference, Fig. 2D). In order to verify the interaction between MIR9-3HG and miR-498, luciferase reporter assay was performed. A significant decrease in luciferase activity was observed following overexpression of miR-498 in C33A and SiHa cells (Fig. 2E).

miR-498 inhibits the expression of EP300. In order to investigate the role of miR-498 in the development of cervical cancer at the molecular level, potential interactions between miR-498 and target proteins were identified using databases (Fig. 3A). A total of six proteins were consistently identified in the PITA (genie.weizmann.ac.il/pubs/mir07/mir07_dyn_data.html), DIANA-microT (diana.cslab.ece.ntua.gr/microT) and miRNAMAP (mirnamap.mbc.nctu.edu.tw) databases: CHORDC1, EIF3J, EP300, LMAN1, GCC2 and DHX35.

The expression of EP300 was significantly decreased in C33A and SiHa cervical cancer cells following miR-498 overexpression (Fig. 3B). Subsequently, miR-498 inhibitor was used to knockdown the expression of miR-498 in C33A and SiHa cells. The expression of miR-498 decreased 2.2-fold following transfection with the inhibitor (Fig. 3C). The expression levels of EP300 and other genes were also detected using RT-qPCR; results showed that the expression of EP300 was increased 2.1-fold following transfection with the miR-498 inhibitor (Fig. 3D). Western blotting was performed to detect the protein levels of EP300 in cervical cancer cell lines. Higher expression levels of EP300 were found in C33A, SiHa, HeLa and CaSki cells, compared with H8 cells (Fig. 3E and F). Furthermore, C33A and SiHa cells expressed relatively higher levels of EP300 compared with HeLa and CaSKi. Additionally, the protein levels of EP300 were significantly inhibited (2-fold) following overexpression of miR-498 in C33A and SiHa cells. Moreover, expression of EP300 was increased following transfection with miR-498 inhibitor (Fig. 3G). These results demonstrated that miR-498 regulated EP300 expression levels. Luciferase reporter assay also showed that luciferase activity decreased following overexpression of miR-498 (Fig. 3H). This suggested that the upregulation of EP300 in C33A and SiHa cells resulted in low miR-498 levels, potentially by reversing the inhibition of EP mRNA translation or the induction of degradation via targeting the 3'untranslated region (UTR) of EP mRNA.

Overexpression of EP300 promotes the proliferation of cervical cancer cells. EP300 was overexpressed in C33A cells. RT-qPCR and western blotting indicated that the mRNA and protein levels of EP300 in C33A cells increased following EP300 overexpression, compared with the control group (1.9-fold; Fig. 4A and B). Subsequently, miR-498 inhibitor and PC-EP300 plasmids were transfected into C33A cells, followed by MIR9-3HG silencing for 24, 48 or 72 h, and cell viability was measured via CCK-8 assay. The viability of C33A cells increased following the inhibition of miR-498 (Fig. 4C). Similarly, the viability of C33A cells was also increased following EP300 overexpression. Additionally, in an EdU assay, the proliferation of C33A cells increased following transfection with the miR-498 inhibitor or EP300 overexpression (Fig. 4D). Thus, miR-498 inhibition EP300 overexpression produced similar effects. Moreover, the inhibition of miR-498 decreased the apoptosis rate of C33A cells; however, EP300 knockdown abolished this effect (Fig. 4E and F).

Knockdown of MIR9-3HG inhibits proliferation of tumors in vivo. In order to validate the mechanism of action MIR9-3HG in cervical cancer *in vivo*, C33A cells with shMIR9-3HG alone or in combination with miR-498 or PC-EP300 transfection were subcutaneously injected into nude mice. The results indicated that MIR9-3HG knockdown inhibited the proliferation of C33A cells *in vivo* (Fig. 5A-C). Tumor volume and weight also decreased following MIR9-3HG knockdown. The maximum tumor diameter and volume were 1.480 cm and 1,513.405 mm^3, respectively. Furthermore, the inhibition of miR-498 rescued the inhibition of tumor growth *in vivo*. Tumor volume and weight were also rescued following miR-498 inhibition or EP300 overexpression. Next, RT-qPCR was performed to measure the expression levels of miR-498 and EP300. The results showed that expression of miR-498 increased following MIR9-3HG knockdown, whereas EP300 overexpression did not significantly alter the levels of miR-498 (Fig. 5D and E), further highlighting EP300 as a downstream molecular effector of miR-498. Furthermore, MIR9-3HG silencing decreased the mRNA and protein levels of EP300, but this effect was reversed following co-transfection with miR-498 inhibitor.

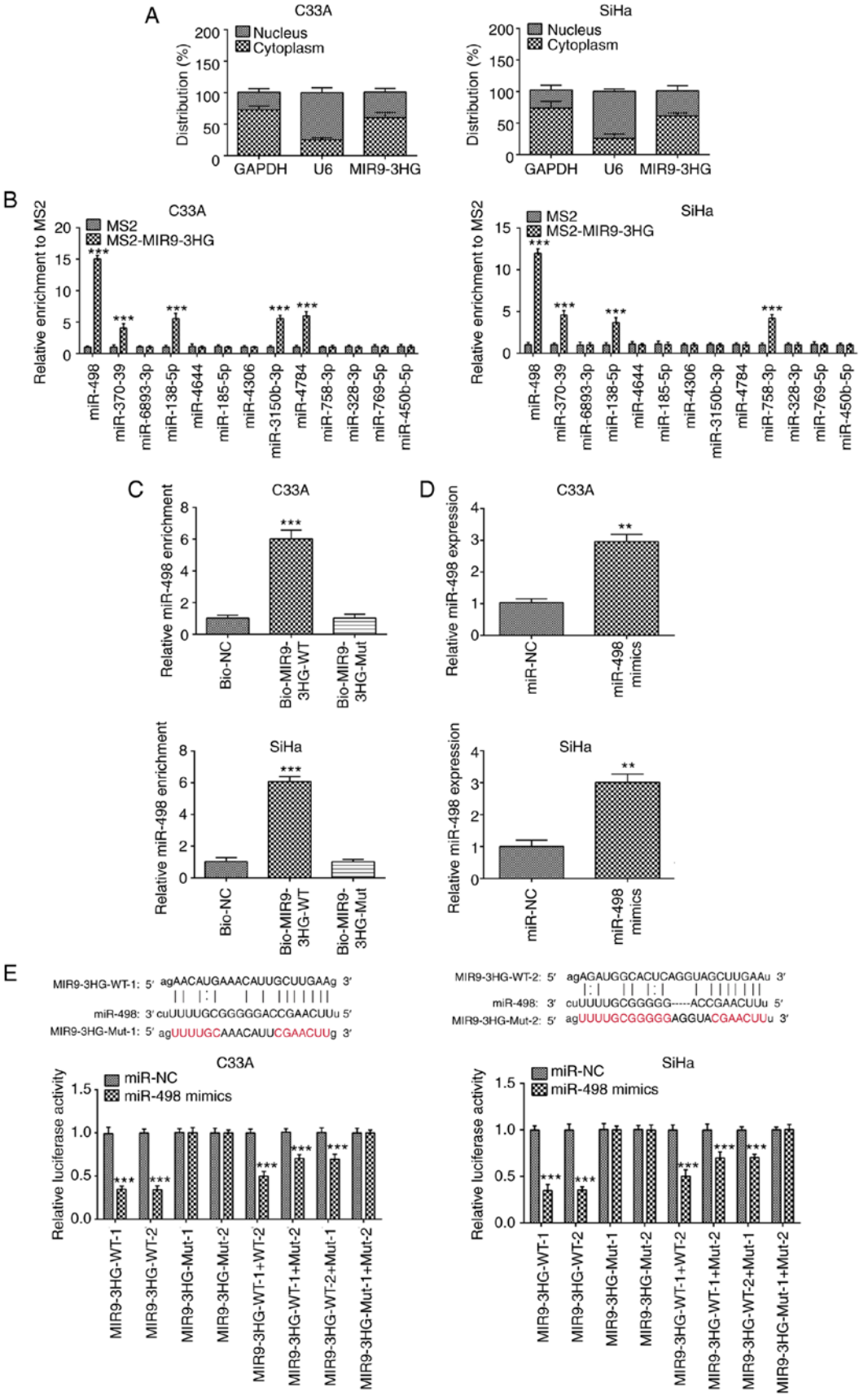

Figure 2. MIR9-3HG targets the 3' untranslated region of miR-498. (A) Expression of MIR9-3HG in cytoplasm and nucleus was detected. (B) Experiments based on MS2 binding sequence-MS2 binding protein. The association between MIR9-3HG and miRs were predicted through Starbase and confirmed by RNA immunoprecipitation assay. ***P<0.001 vs. MS. (C) RNA pull-down assay was performed to detect the association between MIR9-3HG and miR-498 following introduction of Mut MIR9-3HG in C33A and SiHa cells. ***P<0.001 vs. NC. (D) Expression of miR-498 was detected via reverse transcription-quantitative PCR in C33A and SiHa cells following miR-498 mimics transfection. **P<0.01 vs. miR-NC. (E) Predicted binding sites between miR-498 and MIR9-3HG using Starbase and Mut sites of MIR-3HG. Luciferase reporter assays were performed to detect the targeting association between MIR9-3HG and miR-498. Data are presented as the mean ± SD. ***P<0.001 vs. miR-NC. MIR9-3HG, MIR9-3 host gene; miR, microRNA; Mut, mutant; NC, negative control; WT, wild-type.

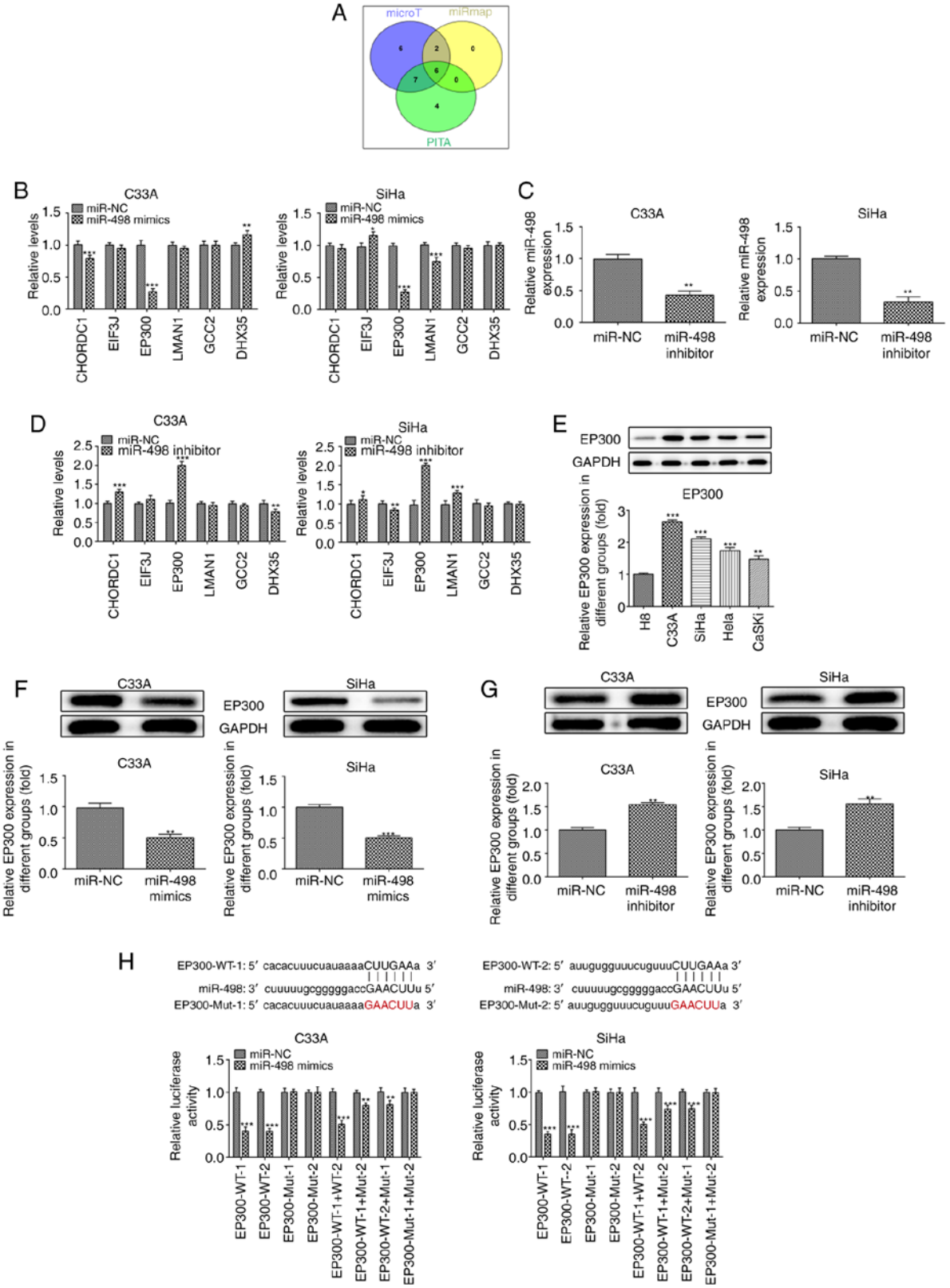

Figure 3. miR-498 targets and inhibits expression of EP300. (A) Target proteins of miR498 were predicted using PITA, DIANA-microT and miRNAMAP databases. (B) mRNA levels of intersection proteins predicted by databases were detected by RT-qPCR in C33A and SiHa cells following miR-498 mimic transfection. *P<0.05, **P<0.01, ***P<0.001 vs. miR-NC. (C) miR-498 inhibitor significantly decreased the levels of miR-498, as detected by RT-qPCR. **P<0.01 vs. miR-NC. (D) miR-498 inhibitor significantly affected the mRNA levels of CHORDC1, EP300 and DHX35, predicted by databases. *P<0.05, **P<0.01, ***P<0.001 vs. miR-NC. (E) Protein levels of EP300 was determined via western blotting in cervical cancer cell lines. **P<0.01, ***P<0.001 vs. H8. (F) miR-498 overexpression significantly decreased the protein levels of EP300 in C33A and SiHa cells. **P<0.01, ***P<0.001 vs. miR-NC. (G) miR-498 silencing significantly increased the protein levels of EP300 in C33A and SiHa cells. **P<0.01 vs. miR-NC. (H) Luciferase reporter assays were performed to validate the target association between EP300 and miR-498. Data are presented as the mean ± SD. **P<0.01, ***P<0.001 vs. miR-NC. miR, microRNA; NC, negative control; RT-q, reverse transcription-quantitative; CHORDC1, cysteine and histidine rich domain containing 1; DHX35, DEAH-box helicase 35; EIF3J, eukaryotic translation initiation factor 3 subunit J; LMAN1, lectin, mannose binding 1; GCC2, GRIP and coiled-coil domain-containing protein; WT, wild-type; Mut, mutant.

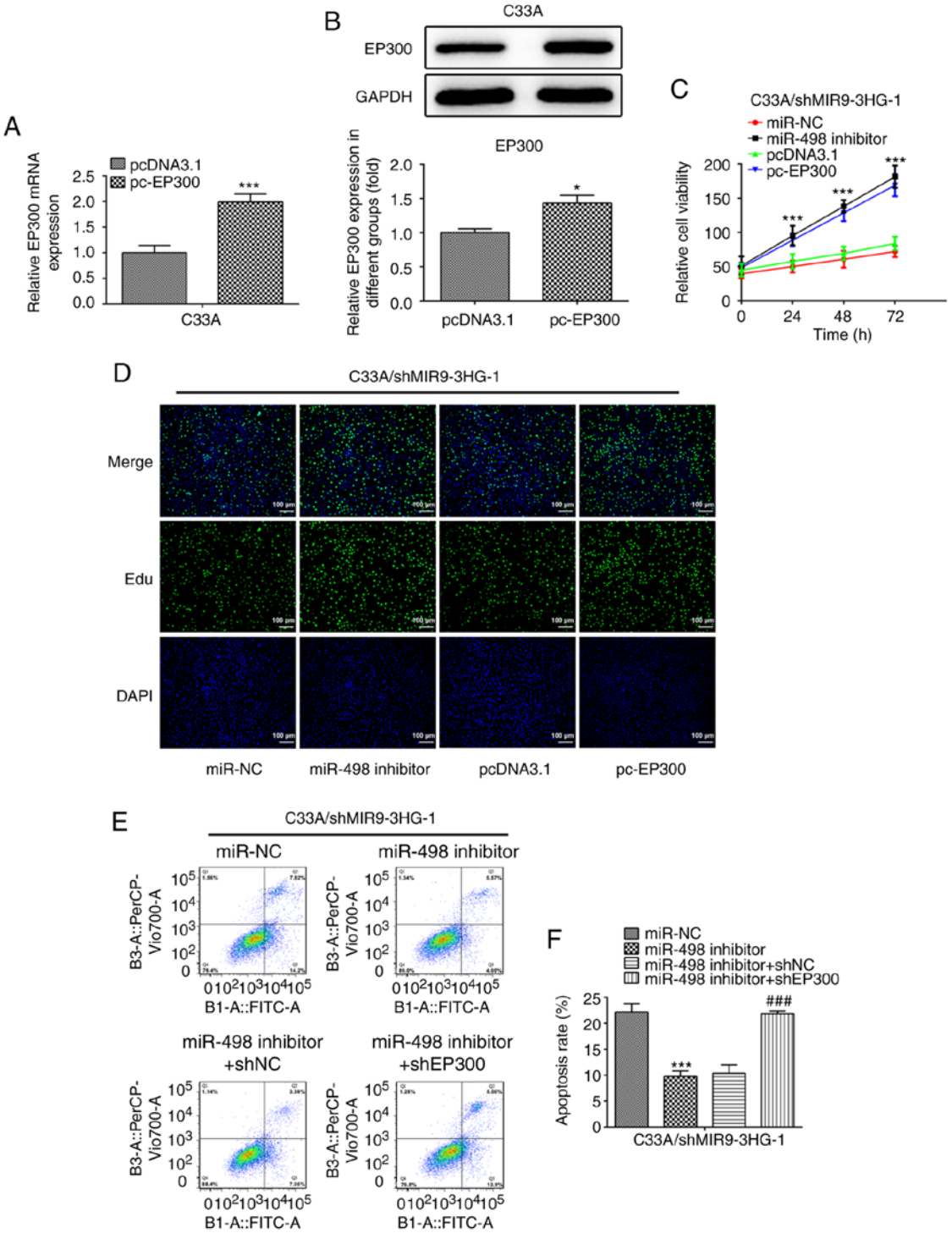

Figure 4. Overexpression of EP300 enhances proliferation and suppresses apoptosis of cervical cancer cells. PC-EP300 upregulated (A) mRNA and (B) protein levels of EP300, as detected via reverse transcription-quantitative PCR and western blotting, respectively. *P<0.05, ***P<0.001 vs. pcDNA3.1. (C) Viability, (D) proliferation and (E and F) apoptosis were determined via Cell Counting Kit-8 and EdU and flow cytometry assay, respectively, following miR-498 inhibition or EP300 overexpression in C33A cells with MIR9-3HG silencing. Magnification, x100. Data are presented as the mean ± SD. ***P<0.001 vs. miR-NC or pcDNA3.1. $^{\#\#\#}$P<0.001 miR-498 inhibitor + shNC. EdU, 5-ethynyl-2'-deoxyuridine; miR, microRNA; MIR9-3HG, MIR0-3 host gene; NC, negative control; sh, short hairpin.

The levels of Ki-67 in tumors were also determined via western blot analysis. Expression levels of Ki-67 were decreased following MIR9-3HG knockdown, which was reversed following inhibition of miR-498 or overexpression of EP300 (Fig. 5E). This suggested that Ki67 expression was regulated via the MIR9-3HG/miR-498/EP300 axis.

Discussion

Cervical cancer is one of the most common types of gynecological malignancy and one of the leading causes of mortality in women with cancer (15). Studies have shown that cervical cancer cells invade and metastasize in the body, leading to poor

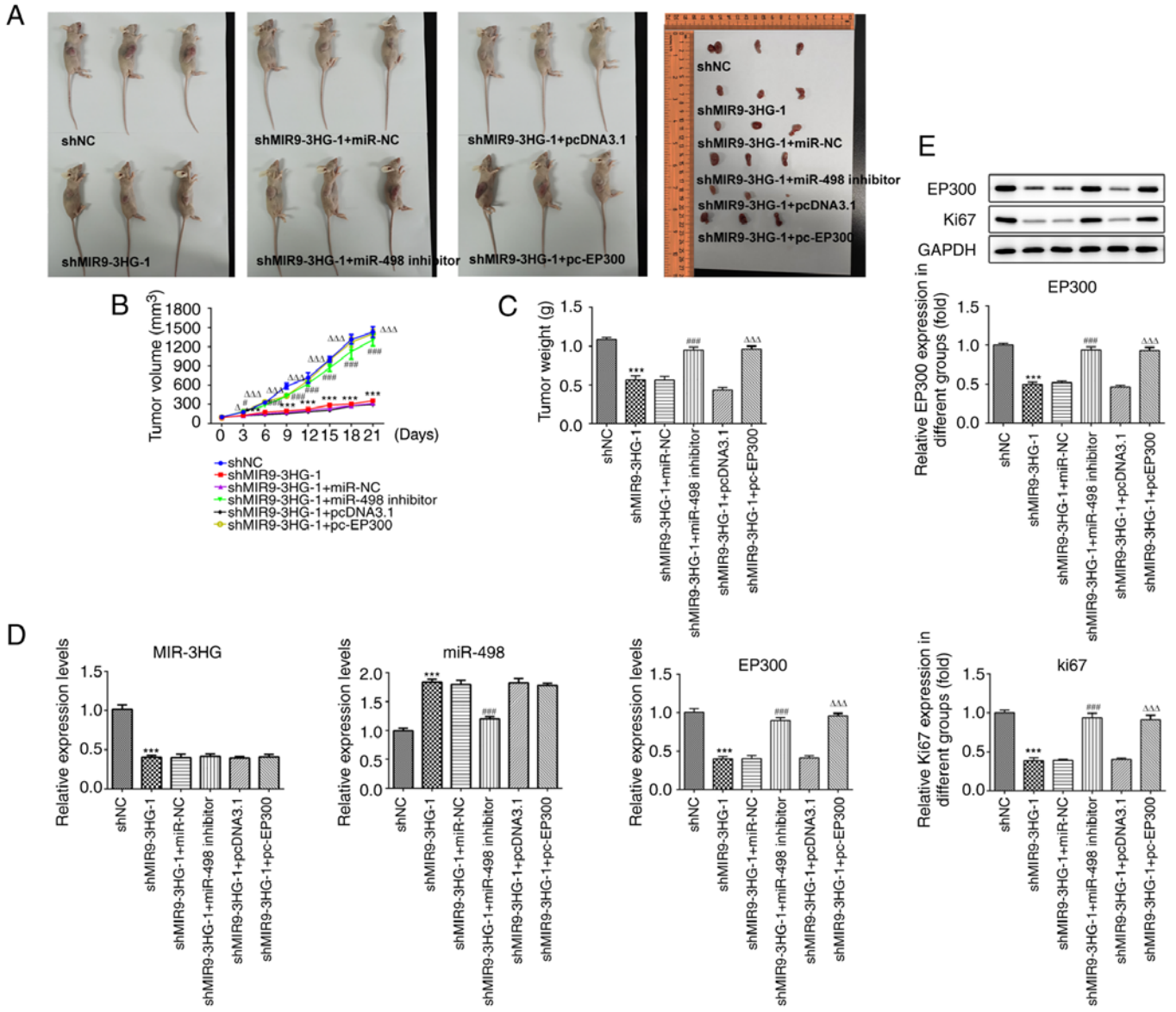

Figure 5. Knockdown of MIR9-3HG suppresses proliferation of cervical cancer cells *in vivo*. (A) Mice were subcutaneously injected with C33A cells with different transfection treatment. (B) Tumor volume was detected every three days. (C) Tumor weight was measured after 21 days. Expression levels of (D) miR-498 and EP300 mRNA and (E) EP300 and Ki-67 protein in tumors were detected via reverse transcription-quantitative PCR and western blotting, respectively. Data are presented as the mean ± SD. ***P<0.001 vs. shNC. $^{###}$P<0.001 vs. shMIR9-3HG+miR-NC. $^{\triangle\triangle\triangle}$P<0.001 vs. shMIR9-3HG-1+pc-DNA3.1. MIR9-3HG, MIR9-3 host gene; miR, microRNA; shNC, short hairpin negative control.

prognosis and high mortality (16,17). Although surgery, chemotherapy and radiation therapy can treat >90% of women with early-stage cervical cancer, recurrent and metastatic disease remains the leading cause of cancer-related mortality (18). Therefore, understanding the molecular mechanism underlying the development and occurrence of cervical cancer may provide insight into novel diagnostic criteria and treatment options.

Previous studies have suggested that ncRNA serves a role in the development of cervical cancer (19,20). High levels of MIR9-3HG can induce the development of cervical cancer and are associated with poor prognosis (12). In the present study, MIR9-3HG expression was detected both in the nucleus and cytoplasm of cervical cancer cells. lncRNA expression in the cytoplasm has been implicated in the regulation of mRNA stability and the modulation of translation (21). Another study suggested that lncRNA expression in the nucleus can sponge target miRNA, while cytoplasmic expression can inhibit gene expression via locus-specific histone methylation (22). Therefore, cytoplasmic expression of MIR9-3HG may account for its effect on proliferation and apoptosis in C33A or SiHa cells.

A previous study indicated that expression of MIR9-3HG also promotes the development of head and neck squamous cell carcinoma (13). In the present study, knockdown of MIR9-3HG inhibited the proliferation of cervical cancer cells. Furthermore, silencing MIR9-3HG enhanced apoptosis in these cells. Cell viability increased in a time-dependent manner in the MIR9-3HG silencing group, suggesting that the decrease in the number of cells may be due to inhibition of proliferation and induction of apoptosis. miR-498 affects cell cycle and alters the expression levels of cell cycle-associated proteins, such as cyclin D1 and CDK4 (23-25). Thus, the effect of suppression of MIR9-3HG silencing on cell proliferation may be due to cell

cycle regulation via miR-498. This may also be due to apoptosis induction by MIR9-3HG silencing. Certain studies have showed that miR-498 affects cell apoptosis, potentially via regulating mitochondria-mediated apoptosis-associated proteins, such as caspase-3, Bax and Bcl-2 (26,27). Based on the present results and previous literature, it was hypothesized that the regulation of apoptosis via MIR9-3HG/miR-498 in cervical cancer cells may be mediated by affecting the mitochondria-mediated apoptosis pathway.

The expression of miR-498 is associated with the development of multiple types of cancer, such as cervical cancer and lung cancer (28,29), which affects the proliferation, migration and invasion of cancer cells by regulating the expression levels of certain proteins, such as PTEN and zinc finger E-box binding homeobox 1 (25,30,31). A previous study demonstrated that circular protein arginine methyltransferase 5 regulates the proliferation of non-small cell lung cancer by sponging miR-498 (32). The present study revealed that miR-498 regulated the expression of EP300 by binding to the 3'UTR of EP300 mRNA. Moreover, EP300 mediated the influence of miR-498 inhibitor on promoting proliferation and suppressing apoptosis in C33A cells. High levels of EP300 are associated with the development of several types of cancer (33,34). For example, EP300 enhances the proliferation of breast cancer cells (35). In the present study, a potential targeting association was predicted by searching the PITA, DIANA-microT and miRNAMAP databases, which suggested that miR-498 regulated the expression of EP300. In addition, inhibition of miR-498 abolished the inhibition of proliferation of cervical cancer cells and increased apoptosis mediated by MIR9-3HG knockdown. Moreover, the increased proliferation and decreased apoptosis mediated by the miR498 inhibitor were also reversed following EP300 silencing. Collectively, the present study revealed the regulatory role of the MIR9-3HG/miR-498/EP300 axis on proliferation and apoptosis in C33A cells. Experiments using tumor-bearing mice suggested that the MIR9-3HG/miR-498/EP300 axis served a regulatory role in tumor growth.

The EP300 protein, which is regulated by miRNAs, such as miR-106b and miR25, is a histone acetyltransferase that regulates transcription via chromatin remodeling and serves an important regulatory role in cell proliferation and apoptosis (33,36,37). Moreover, cells express lower levels of Bcl-2 protein following EP300 knockdown, indicating potential involvement of the intrinsic apoptosis pathway (33). The mechanism by which the 3HG/miR-498/EP300 axis regulates apoptosis is still unknown. Further research is required to determine how the MIR9-3HG/miR-498/EP300 axis affects apoptosis in cervical cancer and its potential as a diagnostic markers. In summary, MIR9-3HG may promote proliferation and suppress apoptosis of cervical cancer cells by regulating the expression levels of miR-498 and EP300.

Acknowledgements

Not applicable.

Funding

No funding was received.

Availability of data and materials

The datasets used and/or analyzed during the current study are available from the corresponding author or first author on reasonable request.

Authors' contributions

FL, YL and PY made substantial contributions to the conception and design of the study, acquired, analyzed and interpreted the data, and drafted and revised the manuscript for important intellectual content. FL and PY were responsible for confirming the authenticity of the raw data. All authors read and approved the final manuscript.

Ethics approval and consent to participate

The experiments were approved by the Ethics Committee of the First Affiliated Hospital of Zhejiang Chinese Medical University.

Patient consent for publication

Not applicable.

Competing interests

The authors declare that they have no competing interests.

References

1. Bouvard V, Zaitchouk T, Vacher M, Duthu A, Canivet M, Choisy-Rossi C, Nieruchalski M and May E: Tissue and cell-specific expression of the p53-target genes: Bax, fas, mdm2 and waf1/p21, before and following ionising irradiation in mice. Oncogene 19: 649-660, 2000.
2. Yang L, Yi K, Wang H, Zhao Y and Xi M: Comprehensive analysis of lncRNAs microarray profile and mRNA-lncRNA co-expression in oncogenic HPV-positive cervical cancer cell lines. Oncotarget 7: 49917-49929, 2016.
3. Naga Ch P, Gurram L, Chopra S and Mahantshetty U: The management of locally advanced cervical cancer. Curr Opin Oncol 30: 323-329, 2018.
4. Klingenberg M, Matsuda A, Diederichs S and Patel T: Non-coding RNA in hepatocellular carcinoma: Mechanisms, biomarkers and therapeutic targets. J Hepatol 67: 603-618, 2017.
5. Zhang K, Han Y, Hu Z, Zhang Z, Shao S, Yao Q, Zheng L, Wang J, Han X, Zhang Y, *et al*: SCARNA10, a nuclear-retained long non-coding RNA, promotes liver fibrosis and serves as a potential biomarker. Theranostics 9: 3622-3638, 2019.
6. Lang HL, Hu GW, Zhang B, Kuang W, Chen Y, Wu L and Xu GH: Glioma cells enhance angiogenesis and inhibit endothelial cell apoptosis through the release of exosomes that contain long non-coding RNA CCAT2. Oncol Rep 38: 785-798, 2017.
7. Sandiford OA, Moore CA, Du J, Boulad M, Gergues M, Eltouky H and Rameshwar P: Human Aging and Cancer: Role of miRNA in Tumor Microenvironment. Adv Exp Med Biol 1056: 137-152, 2018.
8. Van Roosbroeck K and Calin GA: Cancer Hallmarks and MicroRNAs: The Therapeutic Connection. Adv Cancer Res 135: 119-149, 2017.
9. López-Urrutia E, Bustamante Montes LP, Ladrón de Guevara Cervantes D, Pérez-Plasencia C and Campos-Parra AD: Crosstalk Between Long Non-coding RNAs, Micro-RNAs and mRNAs: Deciphering Molecular Mechanisms of Master Regulators in Cancer. Front Oncol 9: 669, 2019.
10. Wang JY, Yang Y, Ma Y, Wang F, Xue A, Zhu J, Yang H, Chen Q, Chen M, Ye L, *et al*: Potential regulatory role of lncRNA-miRNA-mRNA axis in osteosarcoma. Biomed Pharmacother 121: 109627, 2020.

11. Zhang B, Yu L, Han N, Hu Z, Wang S, Ding L and Jiang J: LINC01116 targets miR-520a-3p and affects IL6R to promote the proliferation and migration of osteosarcoma cells through the Jak-stat signaling pathway. Biomed Pharmacother 107: 270-282, 2018.
12. Wu WJ, Shen Y, Sui J, Li CY, Yang S, Xu SY, Zhang M, Yin LH, Pu YP and Liang GY: Integrated analysis of long non coding RNA competing interactions revealed potential biomarkers in cervical cancer: Based on a public database. Mol Med Rep 17: 7845-7858, 2018.
13. Hu Y, Guo G, Li J, Chen J and Tan P: Screening key lncRNAs with diagnostic and prognostic value for head and neck squamous cell carcinoma based on machine learning and mRNA-lncRNA co-expression network analysis. Cancer Biomark 27: 195-206, 2020.
14. Livak KJ and Schmittgen TD: Analysis of relative gene expression data using real-time quantitative PCR and the 2(-Δ Δ C(T)) Method. Methods 25: 402-408, 2001.
15. Jemal A, Bray F, Center MM, Ferlay J, Ward E and Forman D: Global cancer statistics. CA Cancer J Clin 61: 69-90, 2011.
16. Lee YY, Choi CH, Kim TJ, Lee JW, Kim BG, Lee JH and Bae DS: A comparison of pure adenocarcinoma and squamous cell carcinoma of the cervix after radical hysterectomy in stage IB-IIA. Gynecol Oncol 120: 439-443, 2011.
17. Park JY, Kim DY, Kim JH, Kim YM, Kim YT and Nam JH: Outcomes after radical hysterectomy in patients with early-stage adenocarcinoma of uterine cervix. Br J Cancer 102: 1692-1698, 2010.
18. Gupta S, Kumar P and Das BC: HPV: Molecular pathways and targets. Curr Probl Cancer 42: 161-174, 2018.
19. Huang HW, Xie H, Ma X, Zhao F and Gao Y: Upregulation of lncRNA PANDAR predicts poor prognosis and promotes cell proliferation in cervical cancer. Eur Rev Med Pharmacol Sci 21: 4529-4535, 2017.
20. Zhao LP, Li RH, Han DM, Zhang XQ, Nian GX, Wu MX, Feng Y, Zhang L and Sun ZG: Independent prognostic Factor of low-expressed lncRNA ZNF667-AS1 for cervical cancer and inhibitory function on the proliferation of cervical cancer. Eur Rev Med Pharmacol Sci 21: 5353-5360, 2017.
21. Yao RW, Wang Y and Chen LL: Cellular functions of long noncoding RNAs. Nat Cell Biol 21: 542-551, 2019.
22. Katsushima K, Natsume A, Ohka F, Shinjo K, Hatanaka A, Ichimura N, Sato S, Takahashi S, Kimura H, Totoki Y, *et al*: Targeting the Notch-regulated non-coding RNA TUG1 for glioma treatment. Nat Commun 7: 13616, 2016.
23. Li W and Jiang H: Up-regulation of miR-498 inhibits cell proliferation, invasion and migration of hepatocellular carcinoma by targeting FOXO3. Clin Res Hepatol Gastroenterol 44: 29-37, 2020.
24. Lu M, Liu B, Xiong H, Wu F, Hu C and Liu P: *Trans*-3,5,4′-trimethoxystilbene reduced gefitinib resistance in NSCLCs via suppressing MAPK/Akt/Bcl-2 pathway by upregulation of miR-345 and miR-498. J Cell Mol Med 23: 2431-2441, 2019.
25. Zhang X, Xu X, Ge G, Zang X, Shao M, Zou S, Zhang Y, Mao Z, Zhang J, Mao F, *et al*: miR 498 inhibits the growth and metastasis of liver cancer by targeting ZEB2. Oncol Rep 41: 1638-1648, 2019.
26. Chai Q, Zheng M, Wang L, Wei M, Yin Y, Ma F, Li X, Zhang H and Liu G: Circ_0068655 Promotes Cardiomyocyte Apoptosis via miR-498/PAWR Axis. Tissue Eng Regen Med 17: 659-670, 2020.
27. Li G, Tan W, Fang Y, Wu X, Zhou W, Zhang C, Zhang Y, Liu Y, Jiu G and Liu D: circFADS2 protects LPS-treated chondrocytes from apoptosis acting as an interceptor of miR-498/mTOR cross-talking. Aging (Albany NY) 11: 3348-3361, 2019.
28. Rong X, Gao W, Yang X and Guo J: Downregulation of hsa_circ_0007534 restricts the proliferation and invasion of cervical cancer through regulating miR-498/BMI-1 signaling. Life Sci 235: 116785, 2019.
29. Zhao F, Han Y, Liu Z, Zhao Z, Li Z and Jia K: circFADS2 regulates lung cancer cells proliferation and invasion via acting as a sponge of miR-498. Biosci Rep 38: 38, 2018.
30. Duan XM, Liu XN, Li YX, Cao YQ, Silayiding A, Zhang RK and Wang JP: MicroRNA-498 promotes proliferation, migration, and invasion of prostate cancer cells and decreases radiation sensitivity by targeting PTEN. Kaohsiung J Med Sci 35: 659-671, 2019.
31. Liu R, Liu F, Li L, Sun M and Chen K: miR-498 regulated FOXO3 expression and inhibited the proliferation of human ovarian cancer cells. Biomed Pharmacother 72: 52-57, 2015.
32. Wang Y, Li Y, He H and Wang F: Circular RNA circ-PRMT5 facilitates non-small cell lung cancer proliferation through upregulating EZH2 via sponging miR-377/382/498. Gene 720: 144099, 2019.
33. Asaduzzaman M, Constantinou S, Min H, Gallon J, Lin ML, Singh P, Raguz S, Ali S, Shousha S, Coombes RC, *et al*: Tumour suppressor EP300, a modulator of paclitaxel resistance and stemness, is downregulated in metaplastic breast cancer. Breast Cancer Res Treat 163: 461-474, 2017.
34. Attar N and Kurdistani SK: Exploitation of EP300 and CREBBP Lysine Acetyltransferases by Cancer. Cold Spring Harb Perspect Med 7: 7, 2017.
35. Sobczak M, Pitt AR, Spickett CM and Robaszkiewicz A: PARP1 Co-Regulates EP300-BRG1-Dependent Transcription of Genes Involved in Breast Cancer Cell Proliferation and DNA Repair. Cancers (Basel) 11: 11, 2019.
36. Grunstein M: Histone acetylation in chromatin structure and transcription. Nature 389: 349-352, 1997.
37. Bemanian V, Noone JC, Sauer T, Touma J, Vetvik K, Søderberg-Naucler C, Lindstrøm JC, Bukholm IR, Kristensen VN and Geisler J: Somatic EP300-G211S mutations are associated with overall somatic mutational patterns and breast cancer specific survival in triple-negative breast cancer. Breast Cancer Res Treat 172: 339-351, 2018.